Natural Organic Matter (NOM) Imparts Molecular-Weight-Dependent Steric Stabilization or Electrostatic Destabilization to Ferrihydrite Nanoparticles

Zhixiong Li[†1, 2], Sheyda Shakiba[†2], Ning Deng[2], Jiawei Chen[1]*, Stacey M. Louie[2]*, and Yandi Hu[2]*

[1] State Key Laboratory of Biogeology & Environmental Geology, China University of Geosciences, Beijing 100083, PR China

[2] Department of Civil & Environmental Engineering, University of Houston, Houston, TX 77004, United States

† **Equal Contribution**

*Corresponding authors:

Phone and Fax: +86 10 8232678; Email: chenjiawei@cugb.edu.cn

Phone: 713-743-8646; Fax: 713-743-4260; Email: slouie@uh.edu

Phone: 713-743-4285; Fax: 713-743-4260; Email: yhu11@uh.edu

Word count: 6387 text + (4 Figures + 1 Table)*300= 7887 words

TABLE OF CONTENTS FIGURE

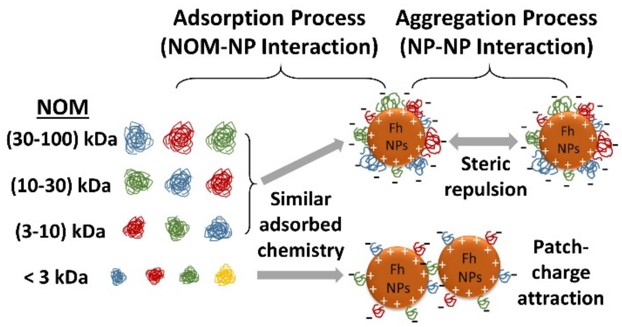

■ ABSTRACT

Ferrihydrite nanoparticles (Fh NPs) are ubiquitous in natural environments. However, their colloidal stability and fate and transport behavior are difficult to predict in the presence of heterogeneous natural organic matter (NOM) mixtures. Here, we investigated the adsorption and aggregation behavior of Fh NPs exposed to NOM fractions with different molecular weights (MW). The NOM fraction with MW < 3 kDa destabilized the NPs, resulting in accelerated aggregation even at high C/Fe mass ratios, whereas higher MW NOM fractions imparted better colloidal stability with increasing MW and C/Fe ratio. Despite differences in the functional group composition of the bulk (dissolved) NOM fractions, all NOM fractions produced similar adsorbed layer compositions on the NPs, suggesting minimal contribution of chemical properties to the distinctive aggregation behavior. Rather, the higher adsorbed mass and larger size of the higher MW fractions were key factors in stabilizing the NPs through steric repulsion, whereas the lowest MW fraction had low adsorbed mass and was unable to counter electrostatic patch-charge attraction when the NPs are positively-charged. This mechanistic understanding helps us predict the transport and fate of Fh NPs and the associated contaminants in natural environments with varying NOM compositions.

■ INTRODUCTION

With iron (Fe) being the fourth most abundant element in Earth's crust, ferrihydrite (Fh, iron hydroxide) nanoparticles (NPs), which can form through precipitation from solution, are ubiquitous in many natural and engineered aquatic environments. Due to their high reactivity and specific surface area, Fh NPs play essential roles in controlling the transport and fate of various aqueous organic and inorganic contaminants.[1-3]

Despite the importance of Fh NPs, their aggregation behavior, which controls the stability, reactivity and transport of the NPs and associated contaminants,[4] is far from well understood. In a recent study by Liu et al., aggregation of Fh NPs was investigated in solutions with varied pH, electrolytes and organic species.[5] However, a detailed evaluation of the effects of natural organic matter (NOM) chemistry and molecular weight (MW) on aggregation of Fh NPs was not reported. NOM is comprised of a complex mixture of biomolecules and their decay products, and hence its interactions with NPs can be difficult to predict. Both the adsorption of NOM and the subsequent effect of adsorbed NOM on interparticle forces must be considered to understand NP aggregation.

For adsorbed mass, the chemical and physical properties of NOM, including functional group composition, charge, and MW, can be important, but contradictory results have been reported in the literature. Li et al. reported that the intermediate MW fractions of SRHA (2-6 kDa) and large SRFA MW fractions (>3.5 kDa) preferentially adsorb onto nano zerovalent iron (nZVI).[6] Other studies have reported preferential adsorption of lower,[7, 8] intermediate,[9] or higher[10-12] MW fractions of NOM onto hematite, goethite, and magnetite. Preferential adsorption of higher MW NOM onto Fh has been reported in some studies[13-15] while Gentile et al. report preferential adsorption of lower MW (i.e., non-colloidal) fractions of soil NOM.[16] Chemical properties can also influence NOM adsorption onto iron oxides. Carboxyl groups are often reported to bind to iron oxides by ligand exchange;[11, 17, 18] preferential adsorption of aromatic species is also commonly reported onto iron oxide particles.[9, 13-15, 17-19]

The preferential adsorption of NOM components with different MWs or chemistries onto Fh NPs will determine the adsorbed mass, layer thickness, chemistry, and charge of the adsorbed NOM, which can all influence the subsequent NP aggregation. A generalized prediction of the effects of NOM on nanoparticles' aggregation behavior can hence be challenging because of the variability in organic matter from different sources. A bottom-up approach has been applied in prior studies[20-25] to compare the effects of MW-fractionated NOM to provide a more fundamental distinction of the role of different NOM components individually and in the complete mixture of NOM, as summarized in the Supporting Information (SI), Table S1. In general, high MW fractions of NOM imparted better colloidal stability for NPs, although two studies showed enhanced flocculation with high MW (> 30 kDa) NOM fractions which was speculated to be caused by bridging with divalent cations[22] or displacement/overcoating of poly(vinyl pyrrolidone) coatings.[23]

Three major knowledge gaps can be identified in the previous studies with MW-fractionated NOM. Firstly, even though the adsorption process of molecular weight fractionated NOM is clearly an important process affecting the aggregation, the adsorption was not thoroughly investigated in the prior studies. Secondly, although electrostatic and steric effects have previously been proposed as controlling mechanisms for aggregation, a detailed characterization of the adsorbed NOM properties was lacking to provide direct evidence. Hence, a major fundamental question could not be answered regarding which properties of the adsorbed NOM, either physical (e.g., surface charge, adsorbed mass, MW of adsorbed species) or chemical (e.g., functional groups, aromaticity) are the main controlling factors in the aggregation process? Finally, only negatively-charged engineered NPs were investigated, whereas iron oxide NPs can be positively-charged at environmentally relevant pH and the charge is susceptible to neutralization or charge reversal by organic ligands such as NOM.[16, 26]

By providing comprehensive characterization of the NOM-NP interactions, this study achieves novel insights into the mechanisms by which NOM imparts either stabilization or destabilization of positively-charged Fh NPs against aggregation.

■ EXPERIMENTAL SECTION

Synthesis and Characterization of Ferrihydrite Nanoparticles. The Fh NP synthesis was modified from the procedure by Tang et al.[27]; detailed information is in the Supporting Information (SI). The stock NP concentration was determined to be 1 g Fe/L by diluting the NP stock 100 times with 2% nitric acid and soaking overnight, followed by quantification by flame atomic absorption spectrometry (AAS, AAnalyst 200, PerkinElmer, Waltham, MA). After drying in a vacuum desiccator at room temperature, the NPs was confirmed to be Fh (SI Figure S1) by X-ray diffraction (XRD) (Miniflex600, Rigaku, Tokyo, Japan). The *z*-average hydrodynamic diameter of the Fh NPs was ≈ 30 nm, as measured in DI water by dynamic light scattering (DLS) using a Malvern Zetasizer Nano ZS instrument (Malvern Instruments, Worcestershire, UK). The isoelectric point (pH_{iep}) of the Fh NPs was determined to be 7.1 (SI Figure S2) by measuring the zeta potential across pH 3 to 10 in 5 mM $NaNO_3$ solution (to impart a consistent ionic strength), using the Smoluchowski fitting model (details in our previous publication[5]). At pH = 5.5, which is the condition used for aggregation and adsorption experiments, the zeta potential was 24.8 ± 1.6 mV (SI Figure S2). DLS was used to determine the aggregation kinetics of Fh NPs in the absence of NOM in solutions containing varied NaCl concentrations (0 to 250 mM) to identify the critical coagulation concentration (CCC), by monitoring the *z*-average hydrodynamic diameter of Fh NPs with a Malvern Zetasizer Nano ZS instrument (Malvern Nano ZS, Malvern, Worcestershire, United Kingdom) every 15 s for 15 min. For each aggregation experiment, 0.5 mL Fh NPs suspension (20 mg Fe/L) was mixed with 0.5 mL NaCl solution with different concentrations, yielding a final NP concentration of 10 mg Fe/L (pH 5.5 ± 0.2). Immediately after mixing, the samples were vortexed for 2 s, inserted into the DLS chamber, and measurement started immediately.

NOM fractionation. To prepare the NOM fractions, 150 mg of Suwannee River NOM (SRNOM) (Cat. No. 1R101N, International Humic Substances Society, St. Paul, MN) was dissolved in 60 mL Milli-Q water. After adjusting pH to 7 with NaOH, the solution was rotated end-over-end overnight at 20 rpm. Then, the solution was filtered through a 0.2 μm PES membrane (EMD Millipore, Burlington, MA) to remove any undissolved SRNOM. A series of Amicon Ultra-15 centrifugal filters (EMD Millipore) with decreasing MW cut-offs (MWCO) of 100 kDa, 30 kDa, 10 kDa, and 3kDa were used for MW fractionation. Filter units were centrifuged at 4714 rpm (4000×*g*) (Eppendorf 5804, Hamburg, Germany) for 10, 30, 40, and 60 min for MWCO 100 kDa, 30 kDa, 10 kDa, and 3 kDa, respectively. All filter units were pre-rinsed by centrifuging with Milli-Q water three times, and the dissolved total organic carbon (TOC) concentration in the final filtrate was negligible (0.42 ± 0.14 mg C/L). Sequential fractionation (schematic in SI Figure S3) was performed to obtain > 100 kDa SRNOM fractions, then 30 to 100 kDa ($\mathrm{SRNOM_{30\text{-}100kDa}}$), 10 to 30 kDa ($\mathrm{SRNOM_{10\text{-}30kDa}}$), 3 to 10 kDa ($\mathrm{SRNOM_{3\text{-}10kDa}}$), and finally < 3 kDa ($\mathrm{SRNOM_{<3kDa}}$). Briefly, the filtrate from each higher MWCO filter was utilized in each following stage of the sequential filtration. The retentate fractions were rinsed in the filter unit with Milli-Q water to remove any remaining lower MW NOM until the filtrate showed minimal observable color, after which the concentrated retentate was recovered and diluted with a measured quantity of Milli-Q water for further use. The concentration as C in each fraction was measured by TOC analysis. The cumulative mass recovery across the entire sequential filtration was ~85%. All stock solutions of fractionated and unfractionated NOM ($\mathrm{SRNOM_{unfractionated}}$) were stored in the dark at 4 °C.

Characterization of MW distributions of NOM. The unfractionated and fractionated NOM were characterized by size exclusion chromatography (SEC) using a Superdex 75 10/300 GL column (GE Healthcare, Chicago, Illinois) on an Agilent 1290 Infinity system (Agilent, Santa Clara, CA) including a binary pump, degasser, autosampler, Agilent 1260 UV−vis diode array detector, DAWN HELEOS II multi angle light scattering (MALS) detector (Wyatt Technology, Santa Barbara, CA), and Optilab T-rEX differential refractive index (dRI) detector (Wyatt Technology). The sample injection volume was 100 μL and flowrate was 0.5 mL/min. In "ideal" SEC theory, analytes do not interact with the stationary phase and elution time corresponds only to the molecular size. However, in practice, NOM shows adsorptive or repulsive interactions with the Superdex column that vary with the ionic strength of the eluent.[20] Therefore, MALS was used to directly quantify MW independently of elution time, using the Zimm model in the Wyatt ASTRA software (7.1.2.5) with the dRI detector as the concentration source (d*n*/d*c* of 0.146 mL/g for SRNOM);[28] details are in the SI. Furthermore, we take advantage of the NOM/column interactions to tune the mobile phase such that each MW fraction elutes within the usable separation and measurement range of the column (between the void volume and solvent volume). For the unfractionated NOM and fractions with MW cutoff > 10 kDa, a mobile phase of phosphate buffer (4 mM, pH 7) with NaCl (25 mM) results in elution of higher MW components after the void volume.[20, 21] For NOM fractions with MWCO < 10 kDa, a lower ionic strength phosphate buffer (2 mM) was chosen to elute low MW components prior to the solvent peak (which produces a negative dRI signal).[20]

Quantification of adsorbed mass of NOM onto Fh NPs. Batch adsorption experiments were performed to investigate the adsorption of unfractionated and fractionated NOM onto Fh NPs (10 mg Fe/L). The adsorbed carbon concentration for samples with initial concentrations of 5 mg C/L or 10 mg C/L in 150 mM NaCl (identified as CCC in the absence of NOM, SI Figure S4) were obtained by solution depletion (measuring the change in carbon concentration due to adsorption) using a TOC analyzer (TOC-L, Shimadzu, Kyoto, Japan). For the $\text{SRNOM}_{\text{<3kDa}}$ fraction, destabilization of the NPs was observed, and an additional sample with an initial NOM concentration of 20 mg C/L was analyzed to further investigate the distinct aggregation behavior.

For sample preparation, the NP stock (1 g Fe/L) was bath sonicated for 30 minutes before sample preparation. Solutions containing NOM and NaCl with a total volume of 6 mL were mixed with 6 mL diluted NP suspensions (20 mg Fe/L) and vortexed for 2 s. The mixture pH was 5.5 ± 0.2 ($n = 15$). To have consistent NP-NOM exposure time with the aggregation experiments (*vide infra*), samples were held at room temperature for 15 minutes. The dissolved (unadsorbed) NOM was isolated from the Fh NPs by centrifuged in an Amicon 100 kDa centrifugal ultrafiltration unit (Millipore Sigma, Burlington, MA) at 4714 rpm (4000×*g*) for 2 minutes (Eppendorf 5804, Hamburg, Germany). Filters were prewashed ten times with NaCl (150 mM), and a total sample volume of 12 mL was filtered. Controls for each NOM type and concentration containing no NPs were prepared with the same procedure, and the adsorbed NOM concentration onto NPs was determined by subtracting the remaining NOM concentration as C in the filtrate of the NP samples from the corresponding NP-free control.

Characterization of adsorptive fractionation of the NOM. To investigate adsorptive fractionation by MW of the NOM onto Fh NPs, SEC-UV_{280} chromatograms (detector wavelength at 280 nm) for each of the NOM fractions were compared before versus after adsorption to NPs. The same solutions prepared for batch TOC measurements (the 100 kDa filtrate for the Fh-NOM mixtures, and the control NOM filtrate with no NPs) were measured using the SEC method reported above.

Additionally, to investigate the possible preferential adsorption of aromatic compounds relative to the TOC,[29] batch UV−vis absorbance spectra of NOM fractions before (filtrate of NP-free control) and after adsorption to NPs (filtrate of the NP-NOM mixtures) were collected using a UV-2600 spectrophotometer (Shimadzu, Columbia, MD). Specific UV absorbances were calculated by dividing the UV absorbance at 280 nm by the TOC concentration.

Finally, to compare the functional groups of the different NOM fractions in the bulk NOM versus those adsorbed to the NPs, ATR-FTIR spectra were collected on a Nicolet iS50 FTIR spectrometer (Thermo Fisher Scientific, Waltham, MA) with a diamond/ZnSe single reflection ATR crystal (PIKE Technologies, Fitchburg, WI). The spectra of the bulk NOM fractions were obtained after drying 6 μL of the NOM solutions (pH ≈ 5.5) onto the ATR crystal. After each set of batch adsorption experiments onto the Fh NPs, the NPs with adsorbed NOM were washed in the centrifugal ultrafiltration units with Milli-Q water to remove any unadsorbed or loosely attached NOM. Then, the NOM-coated Fh NPs were deposited and dried on the ATR crystal. All spectra were acquired from (800 to 4000) cm^{-1} at 2 cm^{-1} resolution, with 200 scans averaged per spectrum and processed by background subtracting the spectrum of the clean ATR crystal.

Fh NPs aggregation and zeta potential measurements with NOM presence. To investigate the effect of NOM on NP aggregation, we conducted similar DLS experiments in the presence of 150 mM NaCl (the CCC value in the absence of NOM) and the unfractionated or fractionated NOM with concentrations of 10 or 5 mg C/L. The aggregation experiments followed the same procedure stated above and the detailed DLS setting can be found in supporting information (SI Section 2.5). The solution containing NaCl and NOM was mixed with an equal volume of Fh NPs suspension. The zeta potentials of the Fh NPs after interacting with NOM were also measured at the end of the 15-min size measurements. We note that although NOM has been reported to self-aggregate or contain ≈ 20 to 30 nm particles for soil humic acids or aquatic NOM in the presence of divalent cations,[30-33] here the light scattering of all SRNOM fractions in 150 mM NaCl is close to the background scattering measured on DI water (both measured with attenuator setting of "11", i.e., the widest aperture), and not significant relative to the aggregating NPs (see SI Section 3.1).

Single-Particle Inductively Coupled Plasma Mass Spectroscopy (spICP-MS). To better understand the fractal structure of the aggregates, DLS measurements of aggregate hydrodynamic diameter were compared to the Fe amount in each aggregate, evaluated as the equivalent spherical NP diameter by spICP-MS. A Thermo Fisher Scientific iCAP RQ quadrupole ICP-MS (ThermoFisher Scientific, Waltham, MA) operating in single particle mode was used for spICP-MS data acquisition, monitoring the ^{57}Fe intensity. For spICP-MS measurement, dilution of the Fh suspensions is required to ensure each recorded spike represents a single aggregate[34-39]. The optimized dilution factors of Fh suspensions were selected at 1000 times, and the measured Fh particle concentrations were in the range of (1 to 5) × 10^5 particles/mL. The spICP-MS analysis was initiated immediately after dilution by Milli-Q water; preliminary tests showed that the dilution process did not lead to rapid dissolution of Fh NPs.

The Fh samples were prepared following the same procedure as the aggregation experiments for DLS measurements, with Fh (10 mg Fe/L) in NOM (10 mg C/L or 5 mg C/L) and NaCl (150 mM) mixed solution. Both the freshly mixed solution and solution after aggregation for 15 min were measured. Based on the measured Fe amount in each aggregate, the particle size was calculated using the chemical structure as $Fe_2O_3 \cdot 2.5H_2O$[27, 40] and a density of 3.8 g/cm^3 for Fh NPs[41] with the spherical-shape assumption. All measurements were repeated three times, average value and standard deviations for particle size and concentration were calculated. Details about spICP-MS measurements and size calculations are in the SI.

Fractal dimension analysis by static light scattering. Static light scattering was also conducted to directly evaluate the fractal dimension of large aggregates in batch samples prepared as for the aggregation experiments. Scattering intensities at various detector angles were measured on a Wyatt DAWN HELEOS II MALS detector and analyzed as reported in prior studies and detailed in the SI.

■ RESULTS AND DISCUSSION

Different MW fractions of SRNOM produce physically distinctive but chemically similar adsorbed layers on Fh NPs

Effect of MW on adsorbed mass and layer thickness

The successful sequential fractionation of SRNOM to produce distinct MW fractions was confirmed by SEC-MALS (chromatograms in Figure S5; average MWs in Table 1). The adsorbed masses and adsorptive fractionation of the SRNOM samples onto the Fh NPs were then evaluated in solution depletion experiments by batch TOC and SEC analysis, respectively. As expected, each NOM fraction produces a higher adsorbed mass at higher C/Fe ratios, $R = 1$, compared to $R = 0.5$ (Figure 1). Furthermore, the adsorbed mass of the SRNOM fractions generally increases with MW, indicating higher adsorbed mass of higher MW fractions of SRNOM to Fh NPs (Figure 1). This result is consistent with preferential adsorption of higher MW NOM onto Fh reported by Lv et al.,[13] Wang et al.,[14] and Coward et al.[15] using electrospray ionization - Fourier transform ion cyclotron resonance mass spectrometry (ESI-FT-ICRMS), and by Ding et al.[18] using fluorescence spectroscopy.

To gain further insight into the adsorption process, SEC-UV_{280} difference chromatograms for the dissolved (unadsorbed) NOM remaining after versus before adsorption were compared (SI Figure S6) to distinguish whether any MW components preferentially adsorb to the Fh NPs. Table 1 compares the weight-averaged MW, M_w, of the adsorbed species to that of the bulk NOM before adsorption. While the more monodisperse $SRNOM_{3\text{-}10kDa}$, $SRNOM_{10\text{-}30kDa}$, and $SRNOM_{30\text{-}100kDa}$ fractions did not show substantial changes in M_w upon adsorption, preferential adsorption of the higher MW components was observed for $SRNOM_{unfractionated}$ and $SRNOM_{<3kDa}$, as is also apparent in the chromatograms (SI Figure S6). This adsorptive fractionation from the more polydisperse samples is consistent with several previous reports for unfractionated NOM adsorbing to iron oxide particles[10-12] and can explain why the unfractionated NOM (containing a broader variety of high and low affinity species) does not fall within the monotonic trend between adsorbed mass and MW observed across the more monodisperse, pre-fractionated NOM (Figure 1). It is noted that Gentile et al. reported that only the small MW fraction of a boreal forest soil extract could adsorb onto the Fh NPs; [16]the difference is likely because the soil extract included very large (> 100 nm) colloidal NOM that did not adsorb, whereas the SRNOM fractions used here (< 100 kDa filtrates, estimated pore size ~9 nm)[42] corresponds to the “small” MW soil NOM that adsorbed.

Finally, the number of adsorbed NOM molecules per Fh NP was estimated (Figure 1, calculations in the SI), using the adsorbed mass from TOC and M_w of the adsorbed NOM from SEC (Table 1). Previously, Tipping found that while the adsorbed mass of humic acids onto goethite increased with MW, the adsorbed number concentrations were similar after normalizing for MW.[12] Here, the estimated number of adsorbed molecules per NP appears to be inversely correlated with the MW of the NOM fraction, in contrast to the trend in adsorbed mass. The higher adsorbed mass for a lower adsorbed number of molecules can suggest a thicker adsorbed layer for the higher MW fractions (schematic in Figure 1), although direct measurements of layer thickness would be required for confirmation. However, advanced techniques such as small angle neutron scattering (SANS) and disc centrifugal sedimentation (DCS), low-energy ion scattering (LEIS), and flow field-flow fractionation (FFF), and may further require the particles to be monodisperse and unaggregated. Hence, direct measurements of layer thickness remain a major challenge.[43]

Effect of functional group composition on adsorbed layer chemistry

Since the chemical composition (particularly aromatic and carboxyl species) has been reported to influence NOM adsorption onto iron oxide NPs,[9, 11, 13-15, 17-19] UV−vis and ATR-FTIR spectroscopy were conducted to explore any differences in functional group composition of the adsorbed species across the NOM fractions. The specific UV absorbance (SUVA) of the bulk NOM fractions (SI Figure S7), which is an indicator of the aromaticity of the NOM,[29, 44] increases with MW up to 100 kDa, consistent with results by Shen et al. for fractionated SRNOM.[22] After interacting with the Fh NPs, SUVA of the unadsorbed NOM was slightly lower than before adsorption (SI Figure S7), consistent with some preferential adsorption of aromatic components, with the largest difference observed for the unfractionated SRNOM.

ATR-FTIR spectra of the unfractionated and fractionated SRNOM before and after adsorption onto Fh NPs were also compared. All SRNOM fractions before adsorption (Figure 2a) show major peaks at 3390 and 1710 cm^{-1} (attributed to the O−H stretch for alcohols and C=O stretch of protonated carboxylic acids (COOH), respectively), 1600 cm^{-1} (aromatic alkenes, conjugated carbonyl, or deprotonated carboxyl groups (COO^{-})), and 1395 cm^{-1} (COO^{-} or the C−O stretch of phenolic groups).[45-49] SRNOM$_{\text{unfractionated}}$ and SRNOM$_{<3\text{kDa}}$ also show an additional peak at 1120 cm^{-1}, attributed to the C−O stretch of alcohols or carbohydrates.[45, 50]

Two changes are observed in the FTIR spectra upon adsorption (Figure 2b): the 1710 cm^{-1} peak is less apparent in the adsorbed NOM on the NPs than the bulk NOM for all of the fractions, and the 1120 cm^{-1} peak in SRNOM$_{\text{unfractionated}}$ and SRNOM$_{<3\text{kDa}}$ does not appear to adsorb substantially to the Fh NPs. These results are consistent with the previously reported participation of carboxyl groups in ligand exchange upon binding to iron oxides[11, 17] (requiring deprotonation of the carboxylic acid), and a relatively low affinity of carbohydrates (reported for some but not all types of NOM[18, 51]). Since the carbohydrate group did not adsorb onto the Fh NPs, the adsorbed NOM coatings appear to have similar functional group compositions regardless of MW (Figure 2b). Prior NP aggregation studies with fractionated NOM were not able to provide chemical characterization of NOM functional groups both *before* and *after* adsorption,[20-24] except for Zhou et al.[25] who only characterize the fractionated NOM after adsorption. Here, although the functional groups of fractionated NOM showed significant difference before adsorption, no significant difference was observed after adsorption. Hence, the NOM layers formed by different MW fractions on the Fh NPs differ primarily in physical properties (adsorbed mass, adsorbed molecular size) rather than chemical properties.

In this section, a comprehensive characterization of adsorbed NOM both before and after adsorption helped us to fill the research gap from the previous studies . The selective adsorption of certain chemical compositions for all NOM fractions could minimize the contribution from chemical properties of fractionated NOM to their effects on NPs' aggregation, as discussed hereafter. Our findings can help understand fractionated NOM effects on other NPs' aggregation.

Characterization of adsorbed NOM discovered the dominant mechanisms

Both inhibition and enhancement of NP aggregation by NOM have been reported.[21-23, 26, 52-54] However, the specific mechanisms by which NOM with different MWs impart differing degrees of NP stabilization are not well understood. Here, detailed characterization of NOM adsorption informs a more mechanistic understanding of aggregation results.

First, CCC of Fh NPs without NOM was determined as ≈ 150 mM NaCl at pH 5.5 (SI Figure S4). This CCC is slightly lower than the reported CCC of 200 mM NaCl at pH = 5.0 ± 0.1 in our previous study,[5] which is consistent with the slightly higher pH in the current study and hence less positive zeta-potential for Fh NPs with pH_{iep} around 7 (SI Figure S2). According to

Derjaguin-Landau-VerweyOverbeek (DLVO) theory, the lowered electrostatic repulsive forces between the less positively charged Fh NPs can result in a lower CCC value, as measured here.

Then, Fh aggregation experiments were conducted at pH = 5.5 in 150 mM NaCl with SRNOM at different C/Fe mass ratios, *R*, of 1 and 0.5 to investigate the effect of NOM on Fh NP aggregation. Figure 3 reports the *z*-average hydrodynamic diameter; the intensity-averaged diameters are provided in SI (S8) along with raw correlation functions (S9) and are consistent with the *z*-average trends in Figure 3.

At both mass ratios, the introduction of $\text{SRNOM}_{<3\text{kDa}}$ unexpectedly resulted in a more rapid increase of size than that observed in the absence of NOM (discussed separately, *vide infra*). On the other hand, the higher MW SRNOM samples were able to stabilize the NPs against aggregation. At $R = 1$ (Figure 3a), the hydrodynamic size of Fh NPs was fully stabilized in the presence of $\text{SRNOM}_{30\text{-}100\text{kDa}}$ and $\text{SRNOM}_{10\text{-}30\text{kDa}}$ and only slightly increased in the presence of $\text{SRNOM}_{\text{unfractionated}}$ (from 67.4 to 84.2 nm) and $\text{SRNOM}_{3\text{-}10\text{kDa}}$ (59.4 to 76.1 nm) during the 15 min measurements. At lower concentrations of SRNOM ($R = 0.5$, Figure 3b), significant inhibition of Fh NPs aggregation is still observed for the highest MW fractions ($\text{SRNOM}_{30\text{-}100\text{kDa}}$ and $\text{SRNOM}_{10\text{-}30\text{kDa}}$). However, $\text{SRNOM}_{3\text{-}10\text{kDa}}$ only partially inhibited NP aggregation, and $\text{SRNOM}_{\text{unfractionated}}$ did not impart any observable stabilization relative to the NOM-free case. These results are consistent with prior reports of NOM fractions with higher MW providing stronger colloidal stabilization of gold and silver NPs than lower MW fractions.[20, 21, 23]

The degree of NP stabilization generally correlates with the adsorbed mass of NOM (Figure 1): NPs with adsorbed masses of > 270 mg C/mg Fe tend to be fully stabilized against aggregation, whereas those with < 200 mg C/mg Fe are not. However, a closer evaluation of the data indicates that adsorbed mass alone cannot fully predict the NP aggregation behavior. Notably, adsorbed masses were similar for $\text{SRNOM}_{\text{unfractionated}}$ at R=1 (230 ± 10 mg C/ g Fe) and $\text{SRNOM}_{3\text{-}10\text{kDa}}$ at R=0.5 (223 ± 14 mg C/ g Fe), but the $\text{SRNOM}_{\text{unfractionated}}$ fully stabilized the NPs whereas $\text{SRNOM}_{3\text{-}10\text{kDa}}$ did not. These NOM coatings differed primarily in the M_w of the adsorbed species

(Table 1). Hence, the larger M_w adsorbed NOM likely produced a thicker layer and imparted stronger steric stabilization.

NOM chemistry has also been postulated to influence NP aggregation, with higher aromaticity correlating to higher adsorption and better stabilization. [55, 56]However, the influences of aromaticity and MW are often indistinguishable because these properties typically co-vary for NOM. Here, differences in SUVA across the MW fractions were less apparent than the differences in MW (for example, comparing $SRNOM_{10\text{-}30kDa}$ to $SRNOM_{30\text{-}100kDa}$, SI Figure S7). Therefore, aromaticity does not appear as important as MW in the adsorption and aggregation process. Furthermore, for the aforementioned case with similar adsorbed masses for $SRNOM_{unfractionated}$ and $SRNOM_{3\text{-}10kDa}$, the $SRNOM_{unfractionated}$ provided enhanced colloidal stability despite having a lower SUVA than $SRNOM_{3\text{-}10kDa}$. Beyond aromaticity, the similarity in the ATR-FTIR spectra of the adsorbed NOM across all MW fractions (Figure 2b) further indicates that the differences in Fh NP aggregation cannot be explained by the functional group composition of the adsorbed NOM.

Finally, electrostatic interactions imparted by the negatively-charged NOM could also affect the aggregation behavior of the Fh NPs. Hence, zeta potential was measured at the end of the aggregation experiments (Figure S10). In all cases, a net charge reversal of Fh NPs from positive to negative was observed after NOM adsorption. However, except for $SRNOM_{<3kDa}$, the zeta potential was generally similar across all NOM fractions, and no significant difference was observed comparing $R = 1$ and 0.5 for each fraction. Therefore, electrostatic interactions could not explain the differences in aggregation behavior for the SRNOM fractions larger than 3 kDa.

While previous studies have also concluded that the higher MW fractions of NOM could provide better stability of NPs (SI Table S1),[20-25] the full characterization of adsorbed mass, adsorptive fractions, and adsorbed layer chemistry presented here provide new, direct evidence to confirm that steric repulsion is the main mechanism by which higher MW SRNOM inhibits the aggregation of Fh NPs at high ionic strengths near the CCC of bare NPs.

Effect of MW-fractionated NOM on <u>positively-charged</u> NPs

In the presence of $SRNOM_{<3kDa}$, instead of inhibiting aggregation, a sudden "jump" of the initial size from 30 nm to ≈ 500 nm occurred under both C/Fe ratios of 1 and 0.5 (Figure 3). While the $SRNOM_{<3kDa}$ adsorption produces a less negative zeta-potential than the other SRNOM fractions, the rapid increase in Fh aggregate sizes in the presence of $SRNOM_{<3kDa}$ should not be attributable to simple charge neutralization, since the rate of size increase was faster than without NOM at the CCC of 150 mM NaCl, which is presumably the maximum (diffusion-limited) aggregation rate of the Fh NPs by charge screening, following classical DLVO theory. Therefore, the results would not be consistent with simple charge neutralization, as proposed by Gentile et al. to explain Fh NP aggregation by NOM extracted from a boreal forest soil.[16]

We first hypothesized that a higher concentration of $SRNOM_{<3kDa}$ may be able to produce higher adsorbed mass to inhibit aggregation similarly to the other fractions. To test this hypothesis, the C/Fe ratio for $SRNOM_{<3kDa}$ was increased to 2, 5, and 10. However, the rapid size increase occurs even at high C concentrations (SI Figure S11). Adsorption experiments at $R = 0.5$, 1, and 2 showed that the adsorbed mass of $SRNOM_{<3kDa}$ has already plateaued at a maximum of 157 ± 17 mg C/g Fe when $R = 1$ (SI Figure S12), much lower than the adsorbed mass of the higher MW NOM fractions, indicating a low adsorption affinity of $SRNOM_{<3kDa}$.

Secondly, we hypothesized that the rapid jump in the initial hydrodynamic size could be attributed to the formation of a loose "branching" configuration of Fh NP aggregates through a bridging effect by $SRNOM_{<3kDa}$, as has been postulated in other studies to explain an apparent enhanced aggregation observed by DLS.[57-59] DLS measurements could dramatically overestimate the aggregation number (i.e. number of NPs per aggregate) of a "branched" fractal aggregate, due to the use of hydrodynamic size as the basis for aggregate size. To test this hypothesis, spICP-MS was conducted. spICP-MS diameters are expected to be smaller than the DLS hydrodynamic diameters, since spICP-MS directly measures the mass of Fe in each aggregate and then calculates a "diameter" of each aggregate with spherical shape assumption and known density and formula.

This equivalent spherical “diameter” from spICP-MS underestimates the actual physical size, but is more representative of the aggregation number (as reported previously for Au and Ag NPs).[39, 60, 61] The cutoff of the background Fe intensity (measured on deionized water) during the spICP-MS measurement was ≈ 200,000 counts per second (cps) (Figure 4), which would correspond to a Fh NP diameter of ≈ 134 nm (SI eq S2); spikes with intensities higher than 300,000 cps (background + 3 standard deviation) were regarded as single aggregate. The Fh NP aggregate diameter with $\text{SRNOM}_{<3\text{kDa}}$ was 180 ± 20 nm by spICP-MS (SI Figure S13, Table S2). For other conditions without SRNOM or with $\text{SRNOM}_{3\text{-}10\text{kDa}}$, their initial sizes were below the spICP-MS detection limit (134 nm), indicating that no large aggregates formed initially under these conditions, consistent with the DLS measurements. After aggregation for 15 min, particle sizes increased to > 180 nm for the samples without SRNOM, as well as samples with $\text{SRNOM}_{<3\text{kDa}}$ at C/Fe = 1 and $\text{SRNOM}_{3\text{-}10\text{kDa}}$ at C/Fe = 0.5 (SI Figure S13(a), (c), and (d), Table S1), indicating the aggregate mass was high under these conditions.

Additionally, we obtained the fractal dimensions (d_f) of the Fh aggregates by static light scattering. The d_f were 1.8 ± 0.1 and 1.7 ± 0.1 for the samples without SRNOM and containing $\text{SRNOM}_{<3\text{kDa}}$, respectively (Figure S14). This result is consistent with previously reported data around 1.7 suggesting cluster-cluster aggregation in the ferrihydrite NPs[16] and suggests both aggregates formed through electrostatic destabilization rather than NOM-bridging flocculation, which would be expected to produce a lower d_f (looser aggregate structure).[26] The three orthogonal and complementary measurements (DLS, spICP-MS, and static light scattering) all consistently suggest that the rapid increase of the initial DLS size with $\text{SRNOM}_{<3\text{kDa}}$ was due to “true” aggregation of Fh NPs due to electrostatic destabilization, rather than bridging by $\text{SRNOM}_{<3\text{kDa}}$ to form a loose fractal structure.

A possible explanation for these findings is that the negatively-charged $\text{SRNOM}_{<3\text{kDa}}$ forms heterogeneous, “patchy” coatings on the surface of positively-charged Fh NPs, leading to attractive forces between oppositely-charged patches.[62] The acceleration of NP aggregation by patch-charge attraction has previously been reported in the presence of protein,[63] polyelectrolytes[64] and NOM.[26, 65] Prior studies suggested that patch-charge attraction can result in restructuring of hematite NP aggregates over time.[49] Here, the relatively low adsorbed mass of $SRNOM_{<3kDa}$ (Figure 1) compared to the higher MW NOM fractions is consistent with a patchy coating and inability to impart steric repulsion to inhibit NP aggregation. Evaluating Fh aggregation using the higher MW NOM fractions at a lower C/Fe ratio of 0.2 also showed accelerated aggregation (Figure S15), providing corroborating evidence that insufficient adsorbed mass of NOM (resulting in a patchy coating and heterogeneously charged surface) can result in patch-charge attraction. Besides the coverage degree, the patch-charge attraction could also depend on the size of Fh NPs,[62] which proved by investigating the effect of negative charged sulfide (S(-II)) on Fh NPs aggregation. However, this is out of our scope, and further study need to be addressed in the future.

Previous studies reported the inhibition of NP aggregation by $SRNOM_{<3kDa}$ on PVP coated Ag NPs, fullerene or graphene oxide NPs,[22-24] which is opposite to our observation of promoted NP aggregation by $SRNOM_{<3kDa}$ on positively charged ferrihydrite NPs. In these previous studies, the NPs were negatively charged and the reported inhibition mechanisms were enhanced electrostatic repulsion[23] or steric repulsion by negatively charged NOM coatings[22, 24] (Table S1). In contrast, here the < 3 kDa NOM fraction was observed to promote NP aggregation due to the opposite charges of the ferrihydrite NPs and NOM. The observation and mechanisms discovered here may be useful to predict the effect of fractionated NOM on the colloidal stability of other NPs, such as aluminum oxides and TiO_2, that can be positively charged at environmentally relevant pH conditions. Moreover, prior studies reporting patch-charge attraction only used DLS to investigate the aggregation rate,[63-65] here we have demonstrated the first application to our knowledge of spICP-MS and static light scattering in combination with DLS as an effective and novel method to provide stronger evidence distinguishing whether the apparent acceleration of aggregation is attributable to patch-charged attractive forces, rather than bridging. Such method could be adopted for the characterization of other nano-aggregates.

ENVIRONMENTAL IMPLICATIONS

In this study, a systematic characterization of fractionated NOM both before and after adsorption onto NPs was conducted to achieve a solid discussion to rule out or support the various mechanisms that have previously been speculated. To our knowledge, this is the first report of the similarity in adsorbed layer chemistry across different MW fractions of NOM regardless of the difference before adsorption, allowing us to distinguish the importance of the physical properties of the adsorbed NOM (MW and adsorbed mass) over chemical properties in the aggregation process. The MW largely controls the adsorbed mass of SRNOM and subsequent steric stabilization/electrostatic destabilization of the NPs, whereas functional group composition is relatively unimportant. The approach presented here can also be a good guidance for future studies to understand the fate and transport of NPs in natural systems with different NOM compositions.

Furthermore, our study first highlights that the mechanisms by which fractionated NOM stabilizes or destabilizes NPs were significantly different for NPs with opposite charge states to the NOM. For the lowest MW SRNOM species, a low adsorbed mass resulted in accelerated aggregation of the Fh NPs, due to patch-charge attraction between positively charged NP surface and the negatively charged NOM which only partially covers the NPs. Such effects could not occur for the negatively charged NPs. Our unique findings can have broad implications for the effects of fractionated NOM on other positively charged NPs.

Results here can be useful to begin developing semi-empirical models to predict aggregation behavior of Fh NPs in the presence of NOM, given investigation of a wider range of conditions (e.g. pH and ionic strength) and different types of NOM. Given that prior studies observed bridging flocculation by high MW NOM,[22] future studies could investigate the effects of the NOM fractions on positively-charged NPs such as Fh (at pH < 7) with divalent cations such as Ca^{2+}. Additional studies can also investigate the relative influence of MW and chemistry when the NPs are initially coated by large polymers such as polyvinylpyrrolidone (PVP).[23] Thus, detailed characterization of the properties of adsorbed layer could be addressed to explain the mechanisms.

Overall, this knowledge will be critical to understand the transport behavior of Fh NPs and the associated contaminants, which are ubiquitous in natural systems. This research can inspire additional studies to investigate the effect of NOM adsorption on the role of Fh NPs as well as other natural NPs in the colloid-mediated transport of inorganic and organic pollutants in natural environments.

ASSOCIATED CONTENT

Supporting Information

Details about Fh NP characterization, SRNOM fractionation, SEC-MALS analysis, spICP-MS analysis, zeta potential measurements, and additional aggregation data are provided in SI. This information is available at http://pubs.acs.org.

AUTHOR INFORMATION

Corresponding Author

* Emails: chenjiawei@cugb.edu.cn; slouie@uh.edu; yhu11@uh.edu

Notes

The authors declare no competing financial interest.

ACKNOWLEDGMENTS

This material is based upon work supported by the National Natural Science Foundation of China

(No. 41731282, 41472232) and the U.S. National Science Foundation (No. 1705511). Measurement of spICP-MS by Ning Deng was supported by the US Department of Energy (DOE), Office of Science, Basic Energy Sciences, Chemical Sciences, Geosciences, and Biosciences Division and University of Houston High Priority Research Large Equipment Grant. We thank China Scholarship Council for a 1-year fellowship to Zhixiong Li (No. 201806400050). We also thank Michael Harold for use of the FTIR instrument, Gregory V. Lowry for the SEC column, and Charisma Lattao for laboratory assistance.

REFERENCES

1. Michel, F. M.; Ehm, L.; Antao, S. M.; Lee, P. L.; Chupas, P. J.; Liu, G.; Strongin, D. R.; Schoonen, M. A. A.; Phillips, B. L.; Parise, J. B., The structure of ferrihydrite, a nanocrystalline material. *Science* **2007,** *316*, (5832), 1726-1729.
2. Dai, C.; Hu, Y., Fe(III) hydroxide nucleation and growth on quartz in the presence of Cu(II), Pb(II), and Cr(III): metal hydrolysis and adsorption. *Environ. Sci. Technol.* **2015,** *49*, (1), 292-300.
3. Fritzsche, A.; Bosch, J.; Rennert, T.; Heister, K.; Braunschweig, J.; Meckenstock, R. U.; Totsche, K. U., Fast microbial reduction of ferrihydrite colloids from a soil effluent. *Geochim. Cosmochim. Acta* **2012,** *77*, 444-456.
4. Guénet, H.; Davranche, M.; Vantelon, D.; Gigault, J.; Prévost, S.; Taché, O.; Jaksch, S.; Pédrot, M.; Dorcet, V.; Boutier, A.; Jestin, J., Characterization of iron–organic matter nano-aggregate networks through a combination of SAXS/SANS and XAS analyses: impact on As binding. *Environ. Sci. Nano* **2017,** *4*, (4), 938-954.
5. Liu, J.; Louie, S. M.; Pham, C.; Dai, C.; Liang, D.; Hu, Y., Aggregation of ferrihydrite nanoparticles: effects of pH, electrolytes,and organics. *Environ. Res.* **2019,** *172*, 552-560.
6. Li, Z.; Lowry, G. V.; Fan, J.; Liu, F.; Chen, J., High molecular weight components of natural organic matter preferentially adsorb onto nanoscale zero valent iron and magnetite. *Sci. Total Environ.* **2018,** *628-629*, 177-185.
7. Kang, S.; Xing, B., Humic acid fractionation upon sequential adsorption onto goethite. *Langmuir* **2008,** *24*, (6), 2525-2531.
8. Illés, E.; Tombácz, E., The role of variable surface charge and surface complexation in the adsorption of humic acid on magnetite. *Colloids Surf. A Physicochem. Eng. Asp.* **2003,** *230*, (1-3), 99-109.
9. Zhou, Q.; Maurice, P. A.; Cabaniss, S. E., Size fractionation upon adsorption of fulvic acid on goethite: equilibrium and kinetic studies. *Geochim. Cosmochim. Acta* **2001,** *65*, (5), 803-812.
10. Ko, I.; Kim, J.-Y.; Kim, K.-W., Adsorption properties of soil humic and fulvic acids by hematite. *Chem. Speciation Bioavailability* **2005,** *17*, (2), 41-48.
11. Gu, B.; Schmitt, J.; Chen, Z.; Liang, L.; McCarthy, J. F., Adsorption and desorption of different organic matter fractions on iron oxide. *Geochim. Cosmochim. Acta* **1995,** *59*, (2), 219-229.
12. Tipping, E., Adsorption by goethite (α-FeOOH) of humic substances from three different lakes. *Chem. Geol.* **1981,** *33*, (1-4), 81-89.
13. Lv, J.; Zhang, S.; Wang, S.; Luo, L.; Cao, D.; Christie, P., Molecular-scale investigation with ESI-FT-ICR-MS on fractionation of dissolved organic matter induced by adsorption on iron oxyhydroxides. *Environ. Sci. Technol.* **2016,** *50*, (5), 2328-2336.
14. Wang, Y.; Zhang, Z.; Han, L.; Sun, K.; Jin, J.; Yang, Y.; Yang, Y.; Hao, Z.; Liu, J.; Xing, B., Preferential molecular fractionation of dissolved organic matter by iron minerals with different oxidation states. *Chem. Geol.* **2019,** *520*, 69-76.

15. Coward, E. K.; Ohno, T.; Plante, A. F., Adsorption and molecular fractionation of dissolved organic matter on iron-bearing mineral matrices of varying crystallinity. *Environ. Sci. Technol.* **2018,** *52*, (3), 1036-1044.

16. Gentile, L.; Wang, T.; Tunlid, A.; Olsson, U.; Persson, P., Ferrihydrite nanoparticle aggregation induced by dissolved organic matter. *J. Phys. Chem. A* **2018,** *122*, (38), 7730-7738.

17. Han, L.; Sun, K.; Keiluweit, M.; Yang, Y.; Yang, Y.; Jin, J.; Sun, H.; Wu, F.; Xing, B., Mobilization of ferrihydrite-associated organic carbon during Fe reduction: Adsorption versus coprecipitation. *Chem. Geol.* **2019,** *503*, 61-68.

18. Ding, Y.; Liu, M.; Peng, S.; Li, J.; Liang, Y.; Shi, Z., Binding characteristics of heavy metals to humic acid before and after fractionation by ferrihydrite. *Chemosphere* **2019,** *226*, 140-148.

19. Gu, B.; Mehlhorn, T. L.; Liang, L.; McCarthy, J. F., Competitive adsorption, displacement, and transport of organic matter on iron oxide: I. Competitive adsorption. *Geochim. Cosmochim. Acta* **1996,** *60*, (11), 1943-1950.

20. Louie, S. M.; Tilton, R. D.; Lowry, G. V., Effects of molecular weight distribution and chemical properties of natural organic matter on gold nanoparticle aggregation. *Environ. Sci. Technol.* **2013,** *47*, (9), 4245-4254.

21. Louie, S. M.; Spielman-Sun, E. R.; Small, M. J.; Tilton, R. D.; Lowry, G. V., Correlation of the physicochemical properties of natural organic matter samples from different sources to their effects on gold nanoparticle aggregation in monovalent electrolyte. *Environ. Sci. Technol.* **2015,** *49*, (4), 2188-2198.

22. Shen, M.; Yin, Y.; Booth, A.; Liu, J., Effects of molecular weight-dependent physicochemical heterogeneity of natural organic matter on the aggregation of fullerene nanoparticles in mono- and di-valent electrolyte solutions. *Water Res.* **2015,** *71*, 11-20.

23. Yin, Y.; Shen, M.; Tan, Z.; Yu, S.; Liu, J.; Jiang, G., Particle coating-dependent interaction of molecular weight fractionated natural organic matter: impacts on the aggregation of silver nanoparticles. *Environ. Sci. Technol.* **2015,** *49*, (11), 6581-6589.

24. Shen, M.; Hai, X.; Shang, Y.; Zheng, C.; Li, P.; Li, Y.; Jin, W.; Li, D.; Li, Y.; Zhao, J.; Lei, H.; Xiao, H.; Li, Y.; Yan, G.; Cao, Z.; Bu, Q., Insights into aggregation and transport of graphene oxide in aqueous and saturated porous media: Complex effects of cations with different molecular weight fractionated natural organic matter. *Sci. Total Environ.* **2019,** *656*, 843-851.

25. Zhou, Q.; Ouyang, S.; Ao, Z.; Sun, J.; Liu, G.; Hu, X., Integrating biolayer interferometry, atomic force microscopy, and density functional theory calculation studies on the affinity between humic acid fractions and graphene oxide. *Environ. Sci. Technol.* **2019,** *53*, (7), 3773-3781.

26. Amal, R.; Raper, J. A.; Waite, T. D., Effect of fulvic acid adsorption on the aggregation kinetics and structure of hematite particles. *J. Colloid Interface Sci.* **1992,** *151*, (1), 244-257.

27. Tang, Y.; Michel, F. M.; Zhang, L.; Harrington, R.; Parise, J. B.; Reeder, R. J., Structural properties of the Cr(III)−Fe(III) (oxy)hydroxide compositional series: insights for a nanomaterial “solid solution”. *Chem. Mater.* **2010,** *22*, (12), 3589-3598.

28. Shakiba, S.; Hakimian, A.; Barco, L. R.; Louie, S. M., Dynamic intermolecular interactions

control adsorption from mixtures of natural organic matter and protein onto titanium dioxide nanoparticles. *Environ. Sci. Technol.* **2018,** *52*, (24), 14158-14168.

29. Karanfil, T.; Schlautman, M. A.; Erdogan, I., Survey of DOC and UV measurement practices with implications for SUVA determination. *J. Am. Water Works Assn.* **2002,** *94*, (12), 68-80.

30. Xu, F.; Yao, Y.; Alvarez, P. J. J.; Li, Q.; Fu, H.; Yin, D.; Zhu, D.; Qu, X., Specific ion effects on the aggregation behavior of aquatic natural organic matter. *J. Colloid Interface Sci.* **2019,** *556*, 734-742.

31. Österberg, R.; Mortensen, K., Fractal dimension of humic acids. *Eur. Biophys. J.* **1992,** *21*, (3), 163-167.

32. Österberg, R.; Mortensen, K., The growth of fractal humic acids: cluster correlation and gel formation. *Radiat. Environ. Biophys.* **1994,** *33*, (3), 269-276.

33. Österberg, R.; Lindovist, I.; Mortensen, K., Particle size of humic acid. *Soil Sci. Soc. Am. J.* **1993,** *57*, (1), 283-285.

34. Martin, J. D.; Frost, P. C.; Hintelmann, H.; Newman, K.; Paterson, M. J.; Hayhurst, L.; Rennie, M. D.; Xenopoulos, M. A.; Yargeau, V.; Metcalfe, C. D., Accumulation of silver in Yellow Perch (*Perca flavescens*) and Northern Pike (*Esox lucius*) from a lake dosed with nanosilver. *Environ. Sci. Technol.* **2018,** *52*, (19), 11114-11122.

35. Lee, W.-W.; Chan, W.-T., Calibration of single-particle inductively coupled plasma-mass spectrometry (SP-ICP-MS). *J. Anal. At. Spectrom.* **2015,** *30*, (6), 1245-1254.

36. Liu, J.; Murphy, K. E.; MacCuspie, R. I.; Winchester, M. R., Capabilities of single particle inductively coupled plasma mass spectrometry for the size measurement of nanoparticles: a case study on gold nanoparticles. *Anal. Chem.* **2014,** *86*, (7), 3405-3414.

37. Geertsen, V.; Barruet, E.; Gobeaux, F.; Lacour, J.-L.; Taché, O., Contribution to accurate spherical gold nanoparticle size determination by single-particle inductively coupled mass spectrometry: a comparison with small-angle x-ray scattering. *Anal. Chem.* **2018,** *90*, (16), 9742-9750.

38. Hadioui, M.; Merdzan, V.; Wilkinson, K. J., Detection and characterization of ZnO nanoparticles in surface and waste waters using single particle ICPMS. *Environ. Sci. Technol.* **2015,** *49*, (10), 6141-6148.

39. Merrifield, R. C.; Stephan, C.; Lead, J., Determining the concentration dependent transformations of Ag nanoparticles in complex media: Using SP-ICP-MS and Au@Ag core-shell nanoparticles as tracers. *Environ. Sci. Technol.* **2017,** *51*, (6), 3206-3213.

40. Fan, S.; Cao, B.; Deng, N.; Hu, Y.; Li, M., Effects of ferrihydrite nanoparticle incorporation in cementitious materials on radioactive waste immobilization. *J. Hazard. Mater.* **2019,** *379*, 120570.

41. Hiemstra, T.; Van Riemsdijk, W. H., A surface structural model for ferrihydrite I: Sites related to primary charge, molar mass, and mass density. *Geochim. Cosmochim. Acta* **2009,** *73*, (15), 4423-4436.

42. Ladner, D. A.; Steele, M.; Weir, A.; Hristovski, K.; Westerhoff, P., Functionalized nanoparticle

interactions with polymeric membranes. *J. Hazard. Mater.* **2012,** *211-212*, 288-295.

43. Louie, S. M.; Tilton, R. D.; Lowry, G. V., Critical review: impacts of macromolecular coatings on critical physicochemical processes controlling environmental fate of nanomaterials. *Environ. Sci. Nano* **2016,** *3*, (2), 283-310.

44. Li, C.-W.; Benjamin, M. M.; Korshin, G. V., Use of UV spectroscopy to characterize the reaction between NOM and free chlorine. *Environ. Sci. Technol.* **2000,** *34*, (12), 2570-2575.

45. Croue, J.-P.; Korshin, G. V.; Benjamin, M. M., *Characterization of natural organic matter in drinking water*. American Water Works Association: 2000.

46. Max, J.-J.; Chapados, C., Infrared spectroscopy of aqueous carboxylic acids: comparison between different acids and their salts. *J. Phys. Chem. A* **2004,** *108*, (16), 3324-3337.

47. Francioso, O.; Sanchez-Cortes, S.; Tugnoli, V.; Ciavatta, C.; Sitti, L.; Gessa, C., Infrared, raman, and nuclear magnetic resonance (^{1}H, ^{13}C, and ^{31}P) spectroscopy in the study of fractions of peat humic acids. *Appl. Spectrosc.* **1996,** *50*, (9), 1165-1174.

48. Mudunkotuwa, I. A.; Grassian, V. H., Biological and environmental media control oxide nanoparticle surface composition: the roles of biological components (proteins and amino acids), inorganic oxyanions and humic acid. *Environ. Sci. Nano* **2015,** *2*, (5), 429-439.

49. Chen, J.; Gu, B.; LeBoeuf, E. J.; Pan, H.; Dai, S., Spectroscopic characterization of the structural and functional properties of natural organic matter fractions. *Chemosphere* **2002,** *48*, (1), 59-68.

50. Senesi, N.; Miano, T. M.; Provenzano, M. R.; Brunetti, G., Spectroscopic and compositional comparative characterization of I.H.S.S. reference and standard fulvic and humic acids of various origin. *Sci. Total Environ.* **1989,** *81-82*, 143-156.

51. Eusterhues, K.; Rennert, T.; Knicker, H.; Kögel-Knabner, I.; Totsche, K. U.; Schwertmann, U., Fractionation of organic matter due to reaction with ferrihydrite: coprecipitation versus adsorption. *Environ. Sci. Technol.* **2011,** *45*, (2), 527-533.

52. Philippe, A.; Schaumann, G. E., Interactions of dissolved organic matter with natural and engineered inorganic colloids: a review. *Environ. Sci. Technol.* **2014,** *48*, (16), 8946-8962.

53. Liu, J.; Legros, S.; von der Kammer, F.; Hofmann, T., Natural organic matter concentration and hydrochemistry influence aggregation kinetics of functionalized engineered nanoparticles. *Environ. Sci. Technol.* **2013,** *47*, (9), 4113-4120.

54. Ottofuelling, S.; Von der Kammer, F.; Hofmann, T., Commercial titanium dioxide nanoparticles in both natural and synthetic water: comprehensive multidimensional testing and prediction of aggregation behavior. *Environ. Sci. Technol.* **2011,** *45*, (23), 10045-10052.

55. Deonarine, A.; Lau, B. L. T.; Aiken, G. R.; Ryan, J. N.; Hsu-Kim, H., Effects of humic substances on precipitation and aggregation of zinc sulfide nanoparticles. *Environ. Sci. Technol.* **2011,** *45*, (8), 3217-3223.

56. Jiang, Y.; Raliya, R.; Liao, P.; Biswas, P.; Fortner, J. D., Graphene oxides in water: assessing stability as a function of material and natural organic matter properties. *Environ. Sci. Nano* **2017,** *4*, (7), 1484-1493.

57. Liu, X.; Wazne, M.; Chou, T.; Xiao, R.; Xu, S., Influence of Ca^{2+} and Suwannee river humic acid on aggregation of silicon nanoparticles in aqueous media. *Water Res.* **2011,** *45*, (1), 105-112.
58. Luo, M.; Huang, Y.; Zhu, M.; Tang, Y.-n.; Ren, T.; Ren, J.; Wang, H.; Li, F., Properties of different natural organic matter influence the adsorption and aggregation behavior of TiO_2 nanoparticles. *J. Saudi Chem. Soc.* **2018,** *22*, (2), 146-154.
59. Wilkinson, K. J.; Stoll, S.; Buffle, J., Characterization of NOM-colloid aggregates in surface waters: Coupling transmission electron microscopy staining techniques and mathematical modelling. *Fresenius J. Anal. Chem.* **1995,** *351*, (1), 54-61.
60. Chang, Y.-j.; Shih, Y.-h.; Su, C.-H.; Ho, H.-C., Comparison of three analytical methods to measure the size of silver nanoparticles in real environmental water and wastewater samples. *J. Hazard. Mater.* **2017,** *322*, 95-104.
61. El Hadri, H.; Louie, S. M.; Hackley, V. A., Assessing the interactions of metal nanoparticles in soil and sediment matrices–a quantitative analytical multi-technique approach. *Environ. Sci. Nano* **2018,** *5*, (1), 203-214.
62. He, L.; Xie, L.; Wang, D.; Li, W.; Fortner, J. D.; Li, Q.; Duan, Y.; Shi, Z.; Liao, P.; Liu, C., Elucidating the Role of Sulfide on the Stability of Ferrihydrite Colloids under Anoxic Conditions. *Environ. Sci. Technol.* **2019,** *53*, (8), 4173-4184.
63. Sheng, A.; Liu, F.; Xie, N.; Liu, J., Impact of proteins on aggregation kinetics and adsorption ability of hematite nanoparticles in aqueous dispersions. *Environ. Sci. Technol.* **2016,** *50*, (5), 2228-2235.
64. Gillies, G.; Lin, W.; Borkovec, M., Charging and aggregation of positively charged latex particles in the presence of anionic polyelectrolytes. *J. Phys. Chem. B* **2007,** *111*, (29), 8626-8633.
65. Smith, B. M.; Pike, D. J.; Kelly, M. O.; Nason, J. A., Quantification of heteroaggregation between citrate-stabilized gold nanoparticles and hematite colloids. *Environ. Sci. Technol.* **2015,** *49*, (21), 12789-12797.

Tables and Figures

Table 1. Weight-average molecular weight of the SRNOM fractions before and after adsorption.

SRNOM Fractions	NOM Stock Solutions	Adsorption Experiments			
	M_w across the entire distribution[1] (kDa)	M_w across the entire distribution[2] (kDa)		M_w at peak maximum[3] (kDa)	
		Before adsorption	Adsorbed NOM	Before adsorption	Adsorbed NOM
Unfractionated	27.3	25.7	34.4	15.4	24.8
<3 kDa[4]	7.4	8.4	10.3	6.8	8.3
(3-10) kDa	22.4	23.6	24.0	19.0	19.2
(10-30) kDa	42.1	42.3	42.4	34.0	35.2
(30-100) kDa	64.8	61.2	61.3	66.4	62.1

[1] Calculated as $\frac{\sum C_i M_{\mathrm{w},i}}{\sum C_i}$ across the chromatograms in Figure S5, where C_i is the mass concentration from RI detection and $M_{\mathrm{w},i}$ is the weight-averaged molecular weight at each time point i from the Zimm analysis of the MALS data (using RI for concentration).

[2] Calculated as in Footnote 1 for the chromatograms in Figure S6, except estimating C_i from the UV absorbance at 280 nm because of the low RI signal for the 10 mg/L C concentrations used in the experiments; $M_{\mathrm{w},i}$ is based on elution time using the measurements in Figure S5. The raw chromatogram is used for the dissolved NOM before adsorption, and the difference chromatogram for the adsorbed NOM.

[3] Taken as a single M_w at the peak maximum in the chromatograms in Figure S6. The raw chromatogram is used for the dissolved NOM before adsorption, and the difference chromatogram for the adsorbed NOM.

[4] Note adsorptive fractionation observed in the chromatograms (Figure S6) is not apparent here because the lowest molecular weight species produce low MALS signal and are excluded from the M_w analysis.

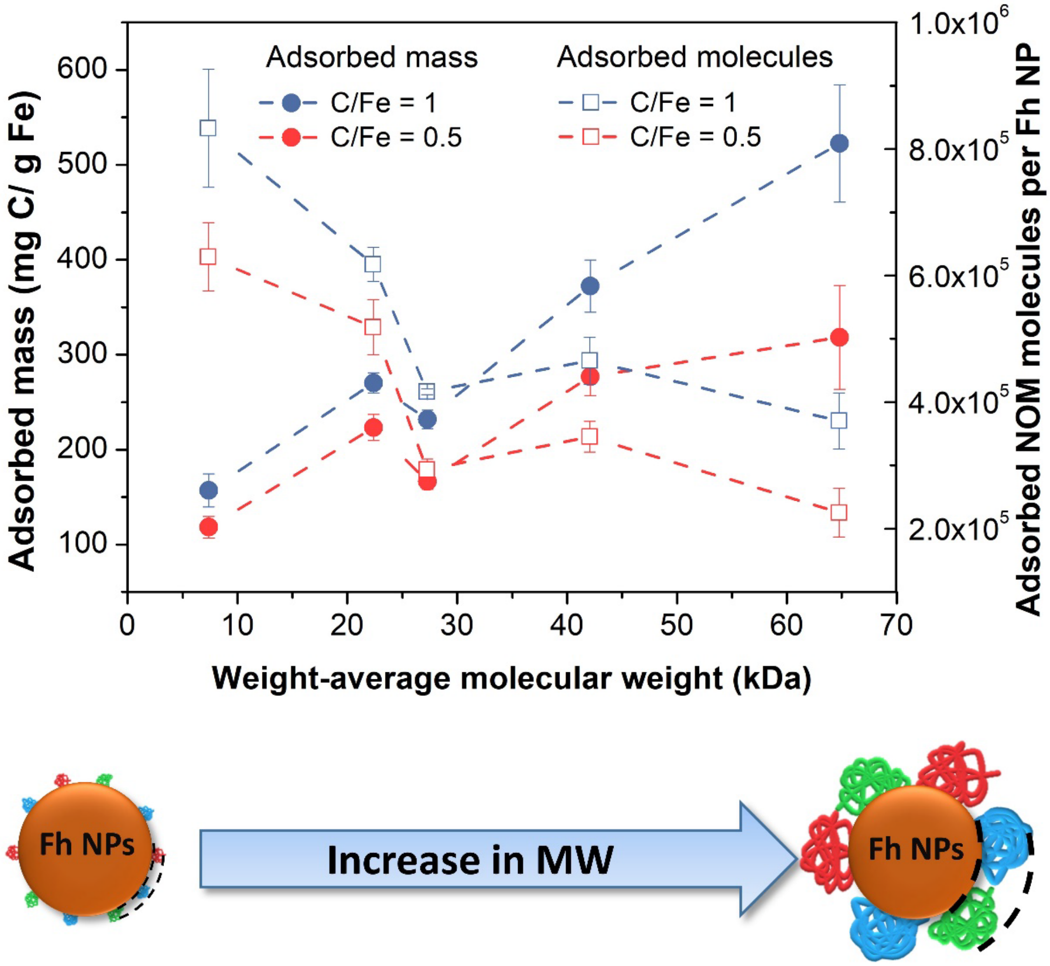

Figure 1. Adsorbed carbon concentration and adsorbed NOM molecules versus weight-average molecular weight of the stock solution of each NOM fraction at *R* = 1 and 0.5. The weight-average molecular weight of $\text{SRNOM}_{<3\text{kDa}}$, $\text{SRNOM}_{3\text{-}10\text{kDa}}$, $\text{SRNOM}_{\text{unfractionated}}$, $\text{SRNOM}_{10\text{-}30\text{kDa}}$, and $\text{SRNOM}_{30\text{-}100\text{kDa}}$ are 7.4 , 22.4, 27.3, 42.1, 64.8 kDa, respectively). Error bars represent the standard deviation of *n* = 2 samples. The lines displayed are only to guide the eye.

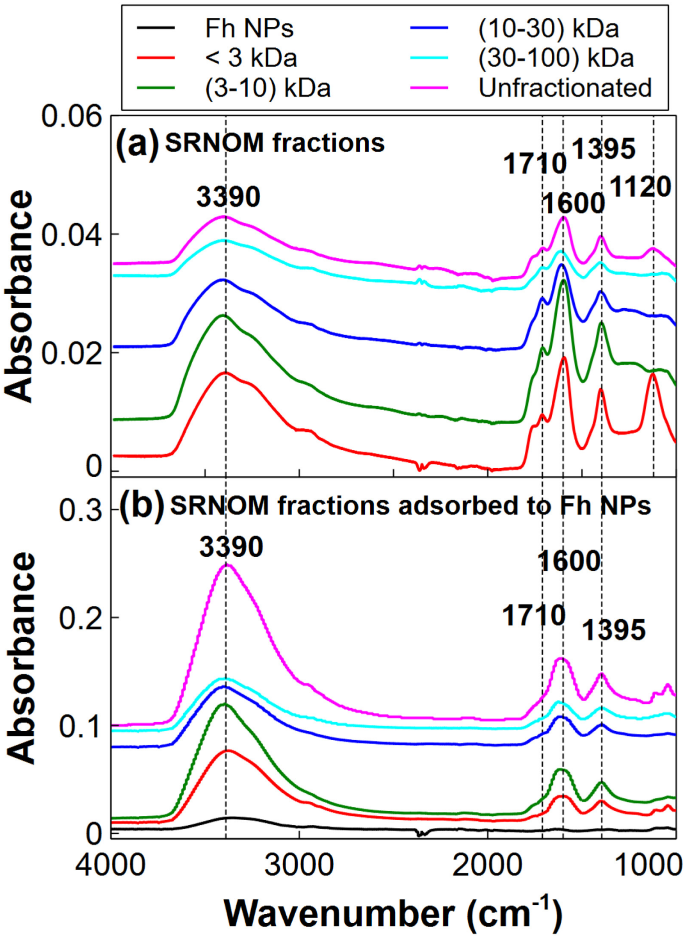

Figure 2. ATR-FTIR spectra for NOM fractions before adsorption (a) and after adsorption onto Fh NPs (b). The spectra for the NOM fractions were obtained by drying 6 μL of the liquid solutions (pH ≈ 5.5) onto the diamond/ZnSe ATR crystal. To collect the NOM-coated NPs, samples were prepared following the same procedure as the batch adsorption experiment and washed with Milli-Q water to remove unadsorbed NOM, then dried onto the ATR crystal. All spectra were acquired from (800 to 4000) cm^{-1} and processed by background subtracting the clean diamond/ZnSe crystal spectrum.

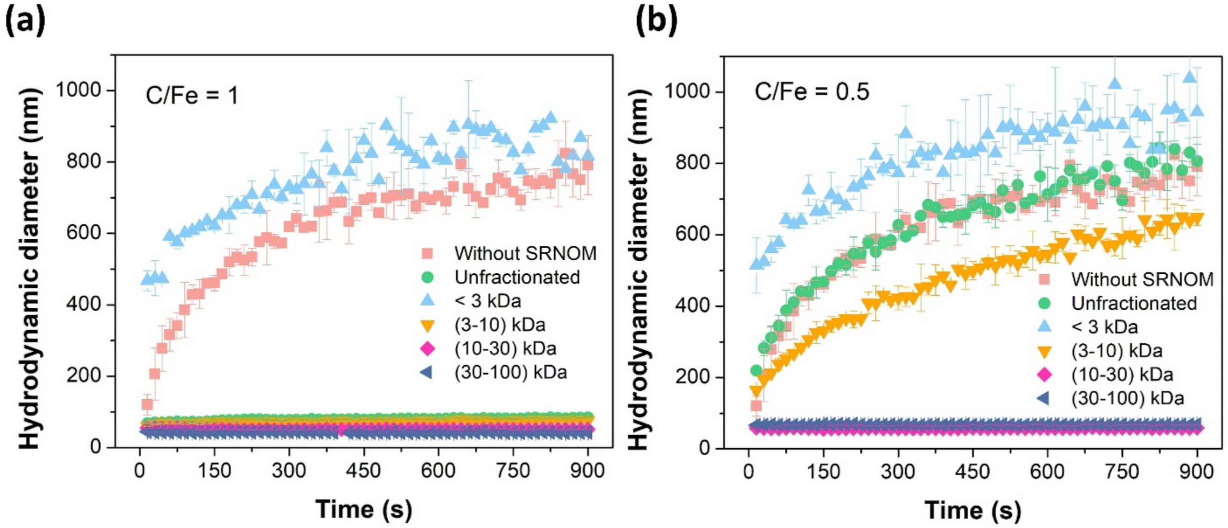

Figure 3. Aggregation kinetic profiles of Fh NPs at pH = 5.5 ± 0.2 in 150 mM NaCl solution, with or without SRNOM (unfractionated or fractionated) with different C/Fe ratios: (a) C/Fe = 1 and (b) C/Fe = 0.5. Error bars represent the standard deviation of n = 2 samples.

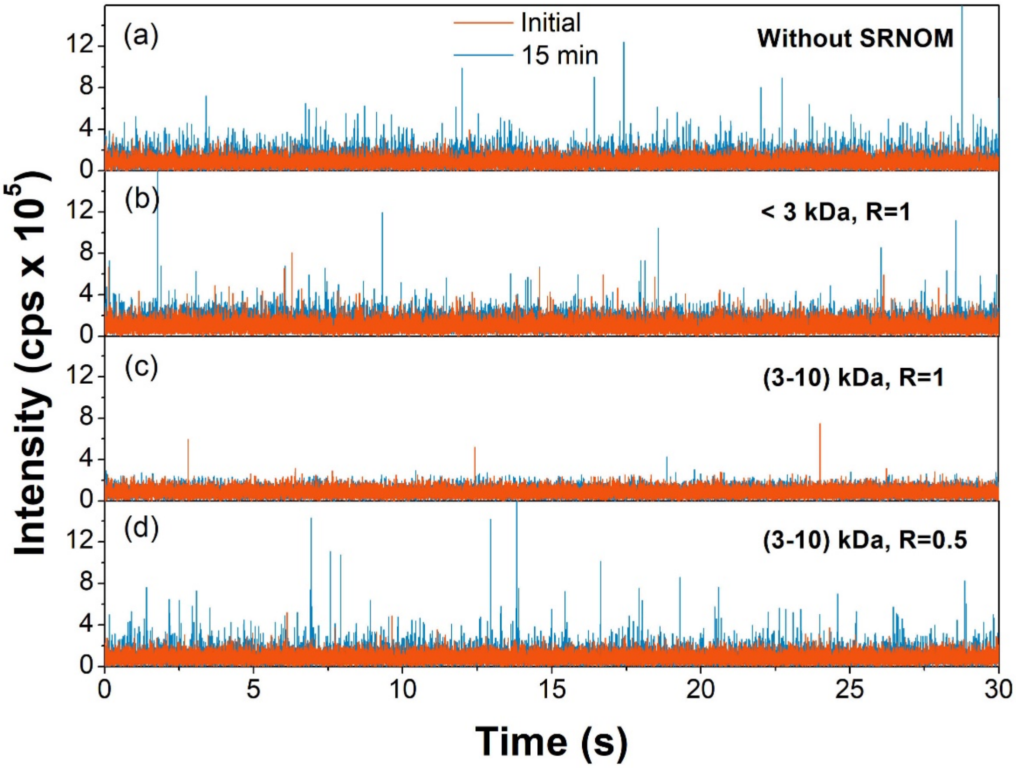

Figure 4. Raw intensity plot of Fh NPs with time scans using spICP-MS. (a) without SRNOM; (b) SRNOM$_{<3kDa}$ C/Fe = 1; (c) SRNOM$_{3-10kDa}$ C/Fe = 1; (d) SRNOM$_{3-10kDa}$ C/Fe = 0.5. Note : The cutoff of the background intensity was selected at 200000 cps, which was corresponding to ~ 134 nm according to eq S2 in SI. Multiple spikes showing up beyond 300000 cps (background + 3σ) for samples (a), (b), and (d) indicating the presence of aggregates larger than 134 nm. More spICP-MS data are available in SI Figure S13.